High-Pressure Three-Phase Fluidization: Hydrodynamics and Heat Transfer

Xukun Luo, Peijun Jiang, and L.-S. Fan
Dept. of Chemical Engineering, The Ohio State University, Columbus, OH 43210

The phase holdups and the heat-transfer behavior were studied experimentally in three-phase fluidized beds over a pressure range of 0.1–15.6 MPa. Bubble characteristics in the bed are examined by direct flow visualization. Pressure effects on the bubble coalescence and breakup are analyzed mechanistically. The study indicates that the pressure affects the hydrodynamics and heat-transfer properties of a three-phase fluidized bed significantly. The average bubble size decreases and the bubble-size distribution becomes narrower with an increase in pressure. The bubble-size reduction leads to an increase in the transition gas velocity from the dispersed bubble regime to the coalesced bubble regime, an increase in the gas holdup, and a decrease in the liquid and solids holdups. The pressure effect is insignificant above 6 MPa. The heat-transfer coefficient between an immersed surface and the bed increases to a maximum at pressure 6–8 MPa and then decreases with an increase in pressure at a given gas and liquid flow rate. This variation is attributed to the pressure effects on phase holdups and physical properties of the gas and liquid phases. A mechanistic analysis revealed that the major heat-transfer resistance in high-pressure three-phase fluidized beds resides in a liquid film surrounding the heat-transfer surface. An empirical correlation is proposed to predict the heat-transfer coefficient under high-pressure conditions.

Introduction

High-pressure operations are common in industrial applications of gas–liquid–solid fluidized-bed reactors for resid hydrotreating, Fischer-Tropsch synthesis, coal methanation, methanol synthesis, polymerization, and other reactions (Fan, 1989). The design and scale-up of these reactors require knowledge of the hydrodynamics and the heat-transfer characteristics of three-phase fluidized beds at high pressures. Although such characteristics have been extensively reported in the literature, most studies were limited to the ambient conditions and little has been reported on high-pressure phenomena with relevance to industrial processes.

The pressure has a significant effect on the hydrodynamic properties of three-phase fluidized beds. The incipient fluidization velocity of three-phase fluidized beds decreases as the pressure increases (Jiang et al., 1995). Tarmy et al. (1984) investigated the hydrodynamic characteristics of three scales of three-phase fluidized beds operated under coal liquefaction conditions ($P = 17.2$ MPa; $T = 450$°C) and two scales under cold conditions ($P = 0.122$–0.621 MPa; $T = 25$°C). They reported that elevated pressures delay the transition from the dispersed bubble to the coalesced bubble regime and increase the gas holdup. Their results showed that the gas holdup in the coal liquefaction conditions can reach as high as 0.5 at a superficial gas velocity of 7 cm/s. A similar high gas holdup (~ 0.5) was reported by Blum and Toman (1977) in a three-phase coal methanator ($P = 6.89$ MPa; $T =$ 100–350°C). Due to the variations of liquid-phase properties and bubble size with pressure, the bed expansion behavior is affected by pressure (Jiang et al., 1996). For a 2.1-mm glass-beads system, increased pressures lead to increased bed expansion, that is, lower solids holdup, while for 1-mm particles, an opposite trend was reported. Only in systems with sintered metal plates or porous plates as the distributor ($P =$ 0.4–1.1 MPa; $T = 143$–260°C; $U_g = 0$–3.5 cm/s), pressure was found to have little effect on the gas holdup (Deckwer et al. 1980).

Although most of the studies attribute the pressure effects to the variation of bubble size with pressure, direct measure-

Correspondence concerning this article should be addressed to L.-S. Fan.

ment of bubble size in three-phase fluidized beds at high pressures is rare. Recently, Jiang et al. (1992) conducted direct flow visualization and reported smaller bubbles with narrower size distributions when the pressure was increased up to 1.0 MPa in a rectangular air–water–glass bead fluidized bed. Similar effects of pressure on the bubble behavior based on flow visualization were reported under both the incipient fluidization and fully fluidized conditions (Jiang et al., 1997) at pressures up to 20 MPa. Two possible reasons for bubble-size variation with pressure were suggested; that is, the increased gas momentum in the bubble-formation process (Tarmy et al., 1984) and the variation of gas–liquid interfacial properties with pressure (Clark, 1990). However, the mechanisms by which the variations in the gas–liquid interfacial properties affect the bubble characteristics have not been fully understood, especially in the coalesced bubble regime where the contribution of the bubble-formation process may not be significant.

Three-phase fluidized beds are characterized by high heat-transfer rate and good temperature controllability. The coefficient of heat transfer between an immersed heating surface and a three-phase fluidized bed under ambient conditions has been measured by a number of investigators (Baker et al., 1978; Kato et al., 1984; Kang et al., 1985; Kim et al., 1986; Magiliotou et al., 1988; Saxena et al., 1989; Kumar et al., 1993a,b; and Kumar and Fan, 1994). Kim and Laurent (1991) provided a review of the wall-to-bed and the heating object-to-bed heat transfer in three-phase fluidization systems. Generally, the heat-transfer coefficient increases with an increase in gas velocity, liquid thermal conductivity and heat capacity, and the size and density of the particles; an increase in liquid viscosity reduces the heat-transfer coefficient. The variation of the heat-transfer coefficient with liquid velocity or bed voidage exhibits a maximum. The heat transfer depends strongly on the hydrodynamics, that is, bubble characteristics and phase holdups. Motion of bubbles can enhance the heat transfer in liquids or liquid–solid suspensions due to bubble-wake-induced turbulence that increases with the bubble size (Kumar et al., 1992). Magniliotou et al. (1988) studied the immersed object-to-bed heat transfer under low and high gas holdup conditions. Surfactants were used to attain the high gas holdups. They found that the heat-transfer coefficient under high gas holdup conditions is always higher than that under low gas holdup conditions. Therefore, the effect of pressure on the heat transfer could be complicated with the bubble-size decrease and the gas holdup increase at high pressures.

Deckwer et al. (1980) conducted the heat-transfer study under coal liquefication conditions ($P = 0.4$–1.1 MPa; $T =$ 143–260°C). No apparent variation of heat-transfer coefficient with pressure was reflected in their experimental data. They also reported that the heat-transfer coefficient can be predicted by extending the correlation for ambient conditions, using the apparent viscosity and the effective thermal conductivity of the liquid–solid medium and the gas holdup under the experimental conditions. These results are consistent with the fact that the pressure does not have a significant effect on the gas holdup in their system, as discussed earlier. However, for systems with significant pressure effect on the hydrodynamics, the effect of pressure on the heat-transfer behavior would be appreciable and simple extrapolation of correlations based on the ambient conditions may not be feasible.

This study examines the effects of pressure on the hydrodynamic and heat-transfer properties of a three-phase fluidized bed. Specifically, the overall or averaged phase holdups and the heat-transfer coefficient between an immersed heating object and the bed are measured over a wide range of pressures. The bubble behavior in the bed is studied based on the flow visualization, and the effect of pressure on the flow transition from the dispersed bubble regime to the coalesced bubble regime is quantified. In addition, the mechanism underlying the heat-transfer phenomenon is discussed and an empirical correlation is proposed to predict the heat-transfer coefficient at high pressures.

Experimental Studies

Experiments are conducted in a high-pressure multiphase flow and visualization system (Figure 1). The maximum operating pressure and temperature of this system are 21 MPa and 180°C, respectively. The system comprises seven main components, the high-pressure fluidized bed, a liquid storage tank, a liquid piston pump, a liquid pulsation damper, a bank of high-pressure gas cylinders, a gas–liquid separation tank, and pressure and temperature control systems. The preheated liquid from the storage tank is driven by the piston pump and fed into the high-pressure fluidized bed. Before the liquid enters the bed, the pulsation is dampened by the liquid pulsation damper. Nitrogen from the high-pressure cylinders (42 MPa) is introduced into the fluidized bed after the pressure and temperature are adjusted to desired values. The gas and liquid streams from the bed flow through a back-pressure regulator and then enter the gas–liquid separation tank, where the gas is vented and the liquid is recirculated. The back-pressure regulator controls the system pressure. The flow rate of the liquid is controlled by adjusting the power of the piston pump. The liquid flow rate is measured

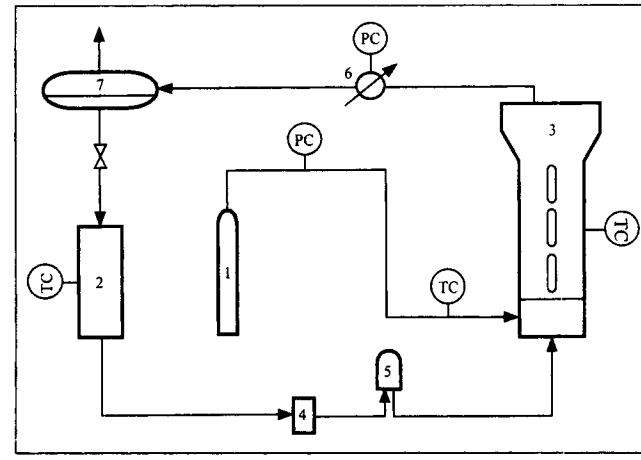

Figure 1. High-pressure three-phase fluidization system.

1. Nitrogen cylinders (408 atm); 2. liquid storage tank; 3. high-pressure three-phase fluidized bed; 4. liquid piston pump; 5. liquid pulsation dampener; 6. back-pressure regulator; 7 gas–liquid separation tank (PC: pressure control; TC: temperature control).

Table 1. Physical Properties of the Paratherm NF Heat-Transfer Fluid*

Properties	Density (kg/m^3)	Viscosity (Pa·s)	Surface Tension (N/m)	Heat Capacity (kJ/kg·K)	Thermal Conductivity (W/m·K)
Values	863	0.018	0.0285	1.926	0.132

*$T = 34°C$; $P = 0.101$ MPa.

by reading the liquid level in the storage tank and is also monitored with a magnetic high-pressure liquid flowmeter. The gas flow rate is measured with either an electromagnetic high-pressure gas flowmeter or three rotameters of various ranges in the gas exhaust line. In this study, Paratherm NF heat-transfer fluid is used as the liquid phase. The physical properties of this liquid are shown in Table 1. Two glass beads of diameters of 2.1 mm and 3 mm ($\rho_s = 2{,}520$ kg/m^3) are used as the solid phase. The bed temperature is controlled at $34 \pm 1°C$ in the experiments.

The detailed structure of the high-pressure three-phase fluidized bed is shown in Figure 2. The bed is a cylindrical stainless-steel column divided into three sections: a plenum section, a test section, and an expansion section. The total height of this column is 800 mm. The lengths of the plenum and the test sections are 100 mm and 500 mm, respectively. The plenum and the test sections have an inside diameter of 50.8 mm. The liquid enters the plenum section through a 12.7-mm stainless-steel tubing at the bottom, and the gas is introduced into the plenum section through a multiorifice sparger. The orifices on the sparger are in a ring arrangement and have a diameter of 3.7 mm. The gas–liquid mixture in the plenum section is distributed into the test section by a perforated plate with 37 square pitched orifices of 2.4 mm diameter. Three pairs of quartz windows are installed on the front and rear sides of the test section through which the bubble characteristics and flow phenomena under high pressure and temperature conditions can be directly observed. The windows have a viewing area of 12.7 mm × 92 mm and are evenly mounted along the test section. The expansion section has a larger inside diameter (101.6 mm) to prevent the entrainment of the particles by the gas and liquid streams. For the same purpose, the gas–liquid stream passes through a copper screen with an opening size of 0.5 mm prior to entering the gas–liquid outlet.

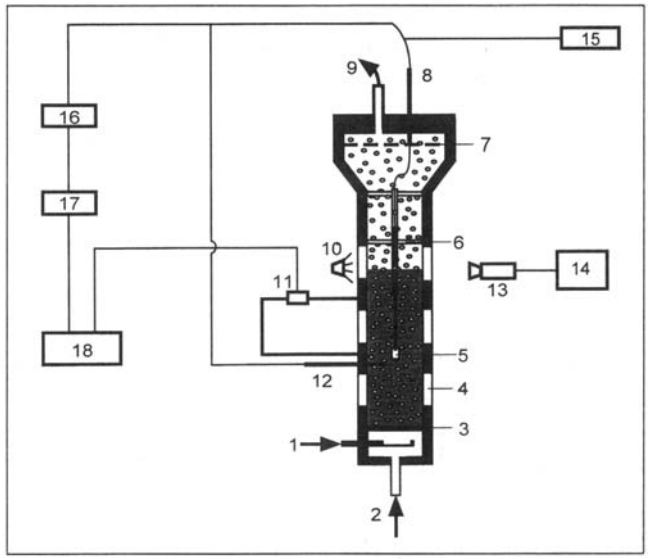

Figure 2. Design and instrumentation for the high-pressure fluidized bed.

1. Gas inlet; 2. liquid inlet; 3. perforated-plate distributor; 4. quartz windows; 5. heat-transfer probe; 6. support of the probe; 7. copper screen; 8. sealing and signal cables; 9. gas and liquid outlet; 10. lighting; 11. differential pressure transducer; 12. thermocouple; 13. video camera; 14. TV and VCR; 15. dc source; 16. signal amplifier; 17. data-acquisition system; 18. computer.

The overall or averaged solids holdup in the bed, ϵ_s, is calculated from a mass balance on the particles:

$$\epsilon_s = \frac{W_s}{\rho_s A H}, \tag{1}$$

where the bed height, H, is obtained by direct visualization. The dynamic pressure gradient in the bed is measured by a differential pressure transducer, and the overall or averaged gas and liquid holdups are determined from the following relationships:

$$\begin{cases} -\dfrac{dP_d}{dz} = \epsilon_s(\rho_s - \rho_l)g - \epsilon_g(\rho_s - \rho_g)g \\ \epsilon_s + \epsilon_l + \epsilon_g = 1. \end{cases} \tag{2}$$

It is noted that, in arriving at Eq. 2, the axial variations of the phase holdups and the fluid–wall friction are neglected. Bubbles emerging from the bed surface are recorded using a video camera with a shutter speed of 1/1,000 s. The images of the bubbles are analyzed to determine the bubble size and bubble-size distribution.

The heat-transfer coefficient is measured with a heat-transfer probe that is designed specifically for high-pressure operations. The probe is placed in the center of the bed (see Figure 2). This probe uses a microfoil heat-flow sensor, which is attached to a dc-powered heater. The design is similar to that used by Kumar et al. (1992). The heat-flow sensor measures directly the local heat flux through the heating surface of the probe by detecting the temperature difference across a thermal barrier of a known thermal resistance. The sensor also detects the temperature of the heating surface. The overall dimensions of this probe are 25.4 × 19.1 × 4 mm. The bulk temperature is measured using a thermocouple (type T) that is placed 15 mm away from the wall, inserted horizontally in the bed. A Das-16 data-acquisition board interfaced with a PC computer digitizes the signals of the heat flux and the temperature difference between the probe surface and the bulk, at a sampling rate of 109 Hz for 18.96 s. In this study, the temperature difference between the heating surface and the bed is maintained at 9°C, unless otherwise specified. Knowing the heat flux and the temperature difference,

the time-averaged heat-transfer coefficient can be calculated from

$$h = \frac{1}{\tau}\int_0^{\tau} \frac{q(t)}{T_s(t) - T_b(t)}\, dt. \tag{3}$$

Results and Discussion

Bubble characteristics and regime transition

Three flow regimes characterize the bubble flow behavior in three-phase fluidized beds: the dispersed bubble regime, the coalesced bubble regime, and the slugging regime. The dispersed bubble regime is characterized by relatively uniform bubble sizes with a small averaged bubble size. In this regime, no bubble coalescence occurs. In contrast, bubbles coalesce in the coalescence bubble regime, and both the bubble size and velocity are large and exhibit wide distributions.

The effect of pressure on the regime transition can be examined through flow observation (Figure 3). It is observed that a few large bubbles and a large number of small bubbles emerge simultaneously from the bed surface in the coalesced bubble regime at low pressures (Figure 3a). As the pressure increases, the emerging frequency and the maximum size of the large bubbles decrease, resulting in the reduction of the average bubble size and the narrowing of the bubble-size distribution. With a further increase in pressure, the large bubbles disappear and bubbles of relatively uniform size are observed, which is characteristic of the dispersed bubble regime (Figure 3b).

The effect of pressure on the regime transition can be elaborated by analyzing the drift flux of gas in three-phase fluidized beds (Figure 4). For gas–liquid flows, the drift flux of gas is defined as the volumetric flux of gas relative to a surface moving at the average velocity of two phases (Wallis, 1969). This definition was extended to three-phase fluidized

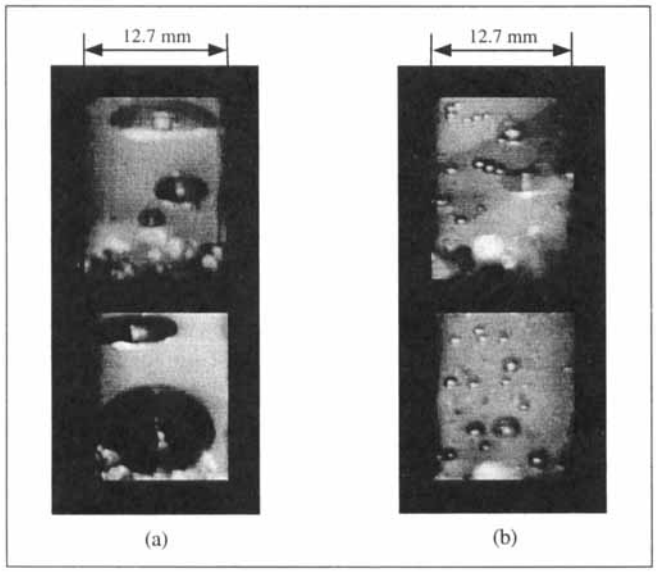

Figure 3. Bubbles under conditions: $d_p = 2.1$ mm; $T = 34$°C; $U_g = 0.7$ cm/s; $U_l = 0.4$ cm/s; (a) $P = 0.79$ MPa; (b) $P = 10$ MPa.

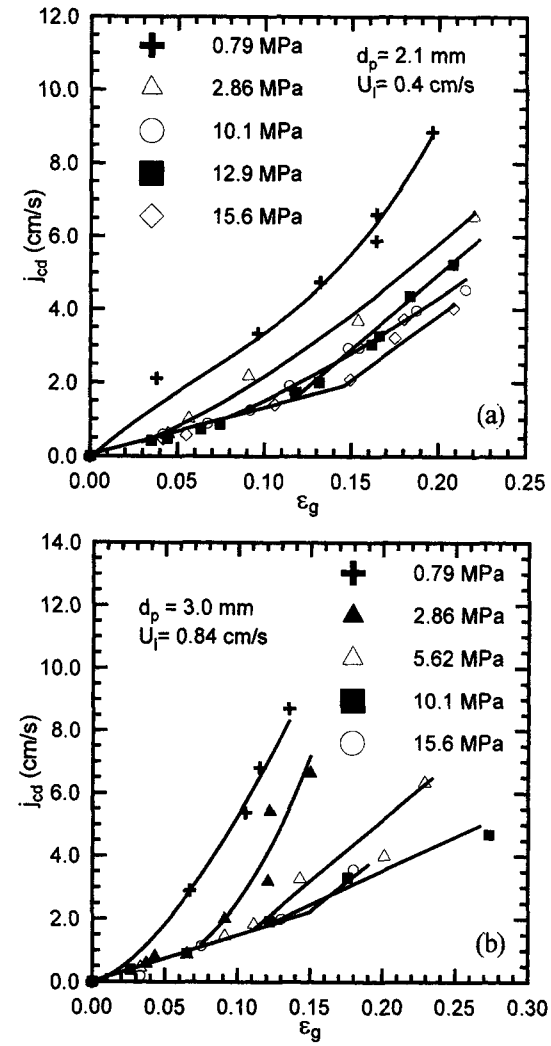

Figure 4. Effects of pressure on the variation of the drift flux with the gas holdup under two conditions: (a) $d_p = 2.1$ mm, $U_l = 0.4$ cm/s; (b) $d_p = 3.0$ mm, $U_l = 0.84$ cm/s.

beds (Darton and Harrison, 1975; Fan, 1989). The drift flux of gas, j_{cd}, in the three-phase fluidized bed can be expressed by

$$j_{cd} = \frac{1-\epsilon_g}{\epsilon_l}(U_g\epsilon_l - U_l\epsilon_g). \tag{4}$$

The drift flux of gas increases with an increase in the gas holdup in the dispersed regime; in the coalesced bubble regime, the rate of increase is much larger. It is clear from Figure 4 that the dispersed bubble regime prevails over a wider range of gas holdups and that the drift flux in the coalesced bubble regime is smaller at a higher pressure. Tarmy et al. (1984) reported that three pilot-scale coal liquefaction reactors operating at $P = 17.3$ MPa and $T = 450$°C with $U_g = 0-7.0$ cm/s, and $\epsilon_g = 0-0.49$ were in the dispersed bubble regime. For two cold units operated over $P = 0.122-0.621$ MPa, they indicated that the regime transition takes place at higher gas holdups as the pressure increases.

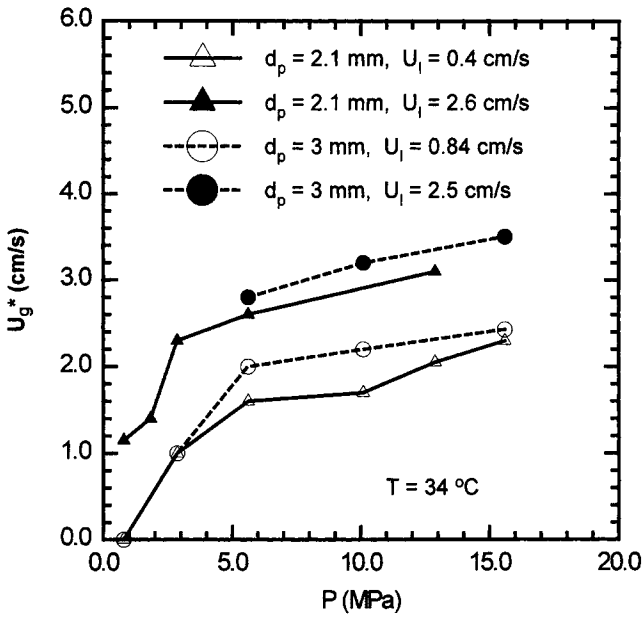

Figure 5. Effect of pressure on the transition gas velocity.

From the relationship between the gas holdup and superficial gas velocity, the gas velocity at the regime transition or the transition gas velocity (U_g^*) can be identified. Figure 5 shows the effect of pressure on U_g^*. As the pressure increases, the transition gas velocity and the gas holdup at transition increase, under all the particle size and liquid velocity conditions. The pressure effect on the regime transition is significant, but the effect levels off at a pressure around 6 MPa. It can also be seen from Figure 5 that U_g^* increases with liquid velocity and slightly with particle size, similar to the regime transition behavior at ambient conditions.

The pressure effect on the flow regime transition is a result of the variation in bubble characteristics. In general, the bubble size and bubble-size distribution are closely associated with factors such as initial bubble size, and bubble coalescence and breakup rates; all of these factors depend on the gas and liquid properties. Bubble behavior is thus affected by pressure since the physical properties of the gas and liquid vary with pressure (see Table 2). Therefore, it is important to examine mechanistically the pressure effect on bubble formation and the rate processes involved in the bubble coalescence and breakup.

Bubble Coalescence. In the coalesced bubble regime, the size of bubbles is closely associated with the rates of bubble coalescence and breakup. For gas–liquid systems, the experimental results available in the literature indicate that an increase of pressure retards the bubble coalescence (Sagert and Quinn, 1977, 1978). There are three steps in the bubble coalescence process (Vrij, 1966; Chaudhari and Hofmann, 1994): (1) approach of two bubbles to form a thin liquid film between them; (2) thinning of the film by the drainage of the liquid under the influence of gravity and suction due to capillary forces; (3) rupture of the film at a critical thickness. The second step is the rate-controlling step in the coalescence process and the bubble coalescence rate can be approximated by the film-thinning rate (Vrij, 1966). The film-thinning velocity can be expressed as (Sagert and Quinn, 1977, 1978)

$$-\frac{dl}{dt}=\frac{8l^3}{3\phi R_d^2\mu_l}\left(\frac{4\sigma}{d_b}+\frac{A_h}{6\pi l^3}\right), \tag{5}$$

where the parameter ϕ is a measure of the surface drag or velocity gradient at the surface due to the adsorbed layer of the gas. Detailed discussion about ϕ is given in Sagert and Quin (1977, 1978). The analysis of the order of magnitude of $4\sigma/d_b$ and $A_h/(6\pi l^3)$ for the present system indicates that the term $A_h/(6\pi l^3)$ can be neglected ($A_h \sim 10^{-20}$, $\sigma \sim 0.02$, $l \sim 10^{-6}$, and $d_b \sim 10^{-3}-10^{-2}$ in SI units).

With increasing pressure, the surface tension decreases and the liquid viscosity increases (Table 2). In addition, ϕ increases with pressure. All these variations contribute to the reduction of the film thinning velocity and hence, the bubble coalescence rate, as the pressure increases. Figure 6a shows the relative film-thinning velocity, the ratio of the film-thinning velocity at a given pressure to that at the ambient pressure. In the calculation, the variations of the physical properties are incorporated and the parameter ϕ is assumed to be constant. From Figure 6a, it can be seen that the film-thinning velocity significantly decreases as the pressure increases. As a result, the time required for two bubbles to coalesce is longer and hence the rate of overall bubble coalescence in the bed is reduced at high pressures. At pressures above 6 MPa, the reduction in the bubble coalescence rate is relatively small. The suppression of bubble coalescence by a pressure increase is even more when the calculation takes into account the increase in ϕ with pressure. Moreover, the frequency of bubble collision decreases with pressure. An important mechanism for bubble collision is bubble wake effects (Fan and Tsuchiya, 1990). When the differences in bubble size and bubble rise velocity are small at high pressures, the likelihood of small bubbles being caught and trapped by the wakes of large bubbles is relatively small. Therefore, the bubble coalesence is suppressed by the increase in pressure, due to the longer bubble coalescence time and the smaller bubble collision frequency.

Bubble Breakup. While the bubble coalescence is suppressed, the bubble breakup is enhanced by an increase in pressure. The pressure effect on the bubble breakup can be

Table 2. Physical Properties of the Gas and Liquid Phases at Various Pressures*

Pressure (MPa)	0.79	2.86	5.62	10.4	12.5	15.6
Gas density (kg/m^3)	8.7	31.3	61.2	114.5	137.1	171.0
Liquid density (kg/m^3)	865	868	872	880	883	891
Liquid viscosity (Pa·s)	0.019	0.022	0.025	0.029	0.030	0.032
Surface tension (N/m)	0.0282	0.0265	0.0252	0.0244	0.0243	0.024

*T = 34°C.

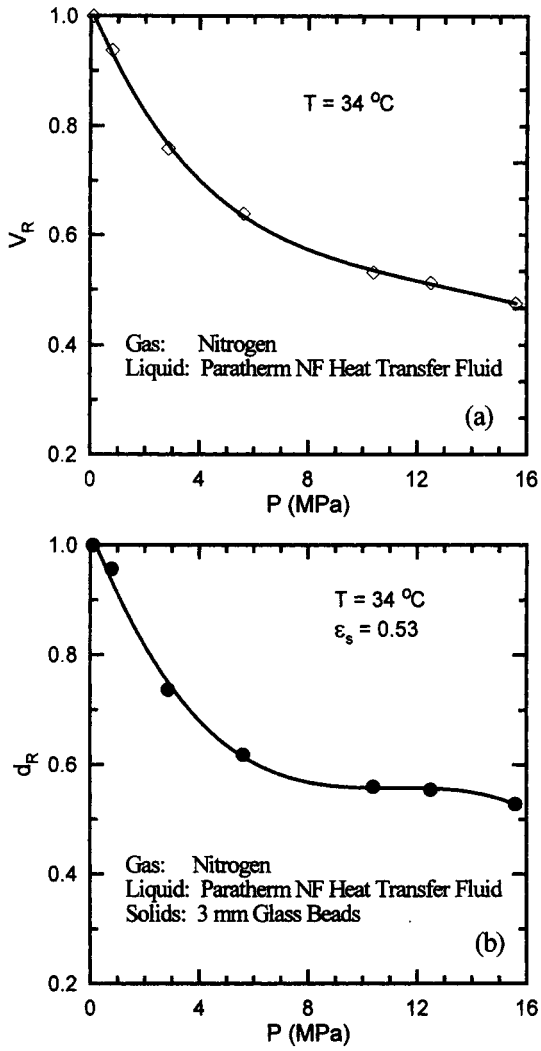

Figure 6. Effects of pressure on: (a) relative film-thinning velocity for two coalescing bubbles; (b) minimum bubble size for particle penetration.

accounted for by considering two mechanisms of bubble breakage, particle–bubble collision and Rayleigh-Taylor instability. Chen and Fan (1989) reported that the penetration of a bubble by a particle upon their collision is the main mechanism for bubble breakup in three-phase fluidized beds. Since the bubble breakup in three-phase fluidized beds is inherently related to the stability of single bubbles, their theory is extended to the analysis of bubble breakup in high-pressure systems. They considered the collision between an ascending spherical cap bubble and a descending particle and established three criteria for particle penetration:

$$\begin{cases} \text{Criterion 1: } a_0 = g\dfrac{\rho_l - \rho_s}{\rho_s} + \dfrac{6\sigma(1 + d_p/2R)}{\rho_s d_p^2} < 0 \\ \text{Criterion 2: } \dfrac{(U_b + U_{p0})\omega}{a_0} > 1 \\ \text{Criterion 3: } \dfrac{a_0 - \left[a_0^2 - (U_b + U_{p0})^2\omega^2\right]^{1/2}}{\omega^2} > H, \end{cases} \tag{6}$$

where

$$\omega = \left(\frac{3}{2}\frac{\rho_l}{\rho_s}\frac{g}{d_p}\right)^{1/2}. \tag{6a}$$

Physically, criterion 1 states that a particle always penetrates a bubble when the initial particle acceleration upon the collision is downwards. Criterion 2 implies that when the particle inertia is sufficient, the particle penetrates a certain depth into the bubble; beyond that depth the liquid head above the particle is so large that the particle continues to penetrate the bubble. Criterion 3 indicates that the particle velocity should be smaller than the ascending velocity of the bubble during the collision process in order for the particle to penetrate the bubble. Since the shape of most large bubbles is close to spherical in the in-bed region (see Figure 3), $2R$ in the preceding equation is approximately equal to the volume-equivalent bubble diameter (d_b). Furthermore, the particle penetration is mainly dictated by first and second criteria in the present experimental system.

Consider a particle–bubble system that does not satisfy any of the criteria just given at the ambient pressure, that is, the particle does not penetrate the bubble. When the pressure increases, the surface tension decreases and the liquid density variation is negligible, resulting in a decrease in a_0 (criterion 1). Hence, criterion 1 could be satisfied at higher pressures for the same particle–bubble system. Meanwhile, the value of $(U_b + U_{p0})\omega/a_0$ increases (criterion 2). Thus, the particle penetration can occur at a pressure that is high enough based on either the first or the second criterion. That is, particles can penetrate and disintegrate smaller bubbles at higher pressures. The minimum bubble size for particle penetration can be calculated based on Eq. 6. Figure 6b shows the values of d_R—the ratio of the minimum bubble size for particle penetration at a given pressure to that at the ambient pressure—at different pressures for the 3-mm particle system. For simplicity, a bubble rise velocity of 7.5 cm/s is employed and the particle velocity is set at zero, based on visual observation and the available experimental data in the literature (Fan and Tsuchiya, 1990). It can be seen from Figure 6b that the bubble breakup by particle penetration is enhanced by a pressure increase. Figures 6a and 6b exhibit a common feature. The pressure effects on both the bubble coalescence and bubble breakup start to level off above a pressure of 6 MPa; this is also the pressure above which pressure does not significantly affect the flow regime transition. This result suggests that the higher transition gas velocities in high-pressure systems are related to the pressure effect on the bubble coalescence and breakup phenomena.

The Rayleigh-Taylor instability concerns the stability of a system in which a fluid is superposed on another fluid of smaller density in a gravitational field. Bubbles may break due to the Rayleigh-Taylor instability on the roof of a bubble (Henriksen and Ostergaard, 1974). It has been suggested that a particle with a diameter greater than half of a critical wavelength (λ_c) generates enough disturbance to break up the bubble (Henriksen and Ostergaard, 1974). The critical wavelength (λ_c) can be calculated from the theory of Bellman and Pennington (1954), expressed by

$$\lambda_c = 2\pi\sqrt{\frac{\sigma}{(\rho_l - \rho_g)g}}. \quad (7)$$

Equation 7 was developed for a plane surface with a two-dimensional sinusoidal disturbance. Chen and Fan (1988) took into account the effect of the curvature of the bubble roof and obtained an equation to calculate λ_c at the nose of the bubble. Their equation has the same form as Eq. 7, except that the coefficient is $2\sqrt{2}\,\pi$ instead of 2π. It is found that λ_c remains virtually constant over the entire pressure range in this study, by employing the physical properties of the fluids at high pressures (σ, ρ_l, and ρ_g; see Table 2) in Eq. 7. The implication is then that the pressure does not affect bubble breakage due to the Rayleigh-Taylor instability.

Bubble Formation. The bubble formation process in the gas distributor also contributes to the bubble size and its distribution in the bed, particularly in the dispersed bubble regime. Most studies on the bubble formation in liquids at high pressures have indicated that, at the same gas flow rates, smaller bubbles are formed at elevated pressures. This is due to an increased gas momentum in the bubble formation process (LaNauze and Harris, 1974; Idogawa et al., 1987).

In summary, the bubble coalescence is suppressed and the bubble breakup by particles is enhanced under high-pressure conditions. Also, the distributor tends to generate smaller bubbles. All these factors contribute to the small bubble sizes and narrow size distributions and, consequently, the flow regime transition characteristics in high-pressure three-phase fluidized beds.

Overall phase holdups

Gas and Liquid Holdups. The gas holdup is affected by the pressure through the variations in the bubble characteristics and the flow regimes. The average bubble rise velocity (based on the volume of bubbles) in three-phase fluidized beds, $\overline{U}_b$, relates to the gas holdup and superficial gas velocity by

$$U_g = \epsilon_g \overline{U}_b. \quad (8)$$

When the distributions of the bubble size and the bubble rise velocity are taken into account, $\overline{U}_b$ can be expressed as

$$\overline{U}_b = \frac{\int_{d_{b,\min}}^{d_{b,\max}} d_b^3 f(d_b) U_b(d_b)\, dd_b}{\int_{d_{b,\min}}^{d_{b,\max}} d_b^3 f(d_b)\, dd_b}. \quad (9)$$

Most of the available correlations of bubble rise velocity in three-phase fluidized beds are given in the form:

$$U_b(d_b) = \eta d_b^{\beta}, \quad (10)$$

where η and β are positive constants ($\beta > 0.5$ for large bubbles) (Fan, 1989). Substituting Eq. 10 into Eq. 9 yields

$$\overline{U}_b = \frac{\int_{d_{b,\min}}^{d_{b,\max}} \eta d_b^{3+\beta} f(d_b)\, dd_b}{\int_{d_{b,\min}}^{d_{b,\max}} d_b^3 f(d_b)\, dd_b}. \quad (11)$$

From this equation, it is clear that the large bubbles would play an important role in detemining the average bubble rise velocity and hence, the gas holdup. $\overline{U}_b$ significantly decreases as the pressure increases at constant gas and liquid velocities because of the decrease in both the number and the size of the large bubbles. From Eq. 8, this results in an increase in the gas holdup in the fluidized beds.

The experimental results of the gas and liquid holdups at different pressures are shown in Figures 7 and 8. The gas holdup at high pressures is always larger than that at low pressures, regardless of the liquid velocity and the particle size. The liquid holdup decreases with an increase in pressure. The pressure effect on the gas holdup is more pro-

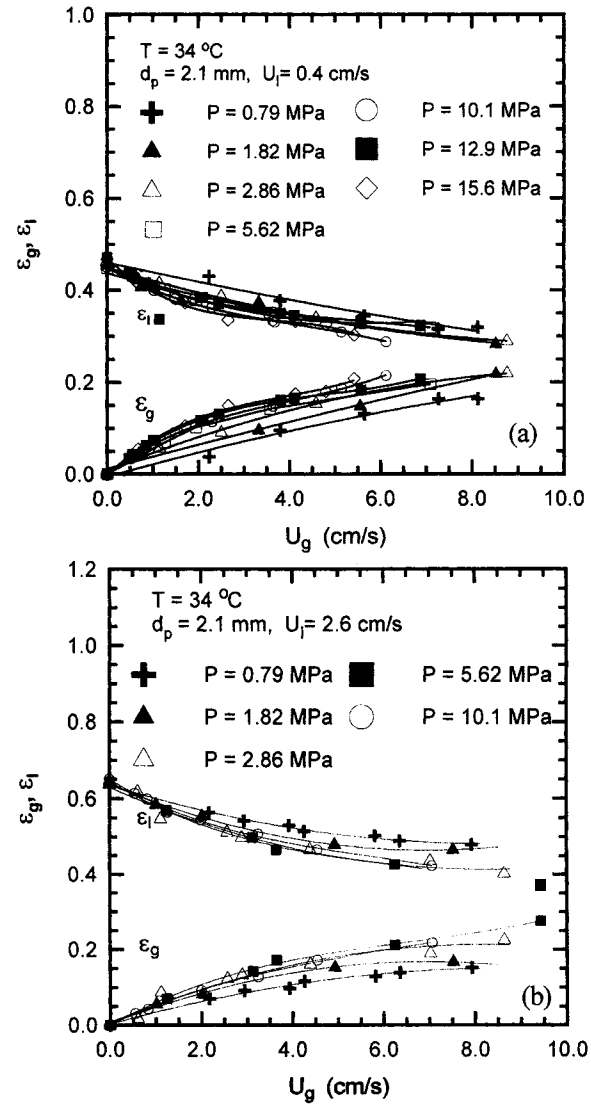

Figure 7. Effects of gas velocity on gas and liquid holdups for d_p of 2.1 mm at various pressures and (a) U_l = 0.4 cm/s; (b) U_l = 2.6 cm/s.

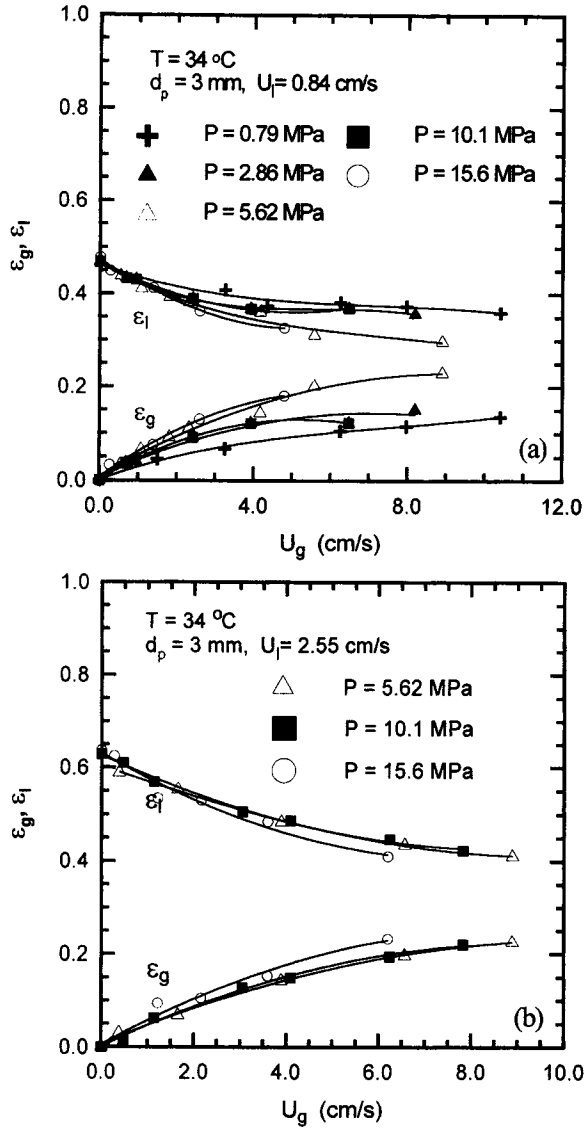

Figure 8. Effects of gas velocity on gas and liquid holdups for d_p of 3 mm at various pressures and (a) $U_l = 0.84$ cm/s; (b) $U_l = 2.55$ cm/s.

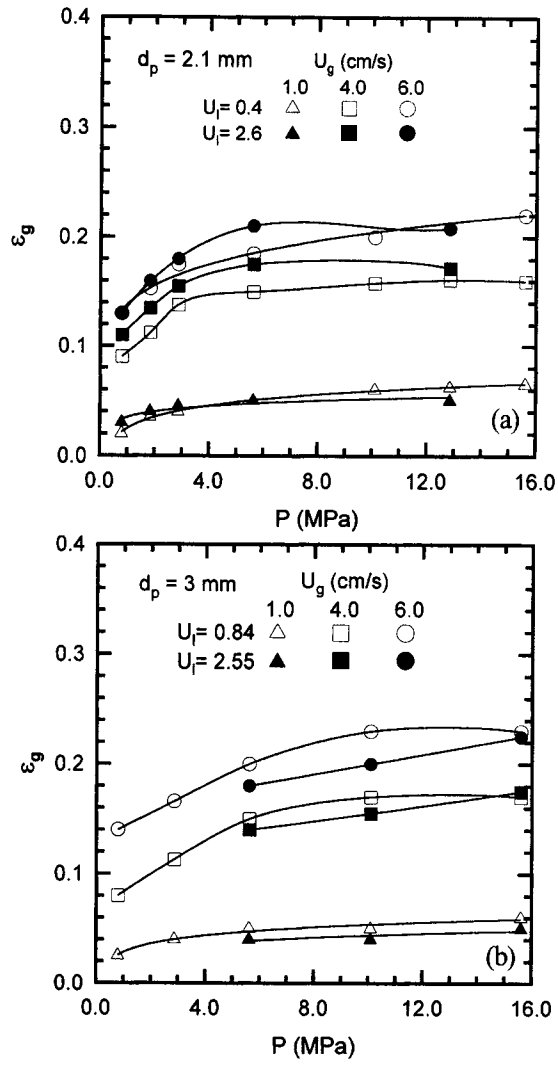

Figure 9. Effects of pressure on gas holdup for various values of U_l, U_g and (a) $d_p = 2.1$ mm; (b) $d_p = 3$ mm.

nounced at high gas velocities. Figure 9 shows the variation of gas holdup with pressure. It is seen that the initial increase in the gas holdup with pressure is significant; when the pressure is above approximately 6 MPa, the increase in gas holdup is substantially reduced. Comparing the results obtained in the 2-mm particle bed and in the 3-mm particle bed, the overall gas holdups in these two systems are similar. However, the gas holdup increases slightly with the liquid velocity for the 2-mm particle system and an opposite trend is observed for the 3-mm particle system.

Solids Holdup. The bed expansion behavior or the solids holdup in three-phase fluidized beds have been extensively studied under ambient conditions (Massimilla et al., 1959; Stewart and Davidson, 1964; Michelsen and Ostergaard, 1970; Bhatia and Epstein, 1974; El-Temtamy and Epstein, 1979). Generally, the solids holdup is more sensitive to the liquid flow rate than to the gas flow rate; the bed always expands with an increase in liquid velocity, independent of the properties of the liquid and solid phases, gas velocities, and bed geometry. Liquid–solid beds can either expand or contract upon the introduction of gas, depending on the particle properties and the liquid velocity. Bed expansion normally takes place in a bed of large/heavy particles; while for fine/light particle systems, the bed contraction occurs. The bed contraction is caused by the entrainment of liquid and particles in the bubble wakes. Figure 10 shows the variation of the solids holdup with the gas velocity at different pressures for the 2.1-mm glass beads. Under the condition of $U_g = 0$, the bed expansion can be described by the Richardson-Zaki equation. Under all the pressure conditions, the bed expands at a liquid velocity of 0.4 cm/s (Figure 10a), but contracts upon the introduction of the gas at a liquid velocity of 2.6 cm/s (Figure 10b). In the entire gas velocity range, the solids holdup decreases with pressure. Figure 11 shows the same trend for the 3-mm particle system as Figure 10a.

The effect of pressure on the solids holdup of three-phase fluidized beds can be attributed to the changes of physical properties of liquid and the bubble characteristics. When the

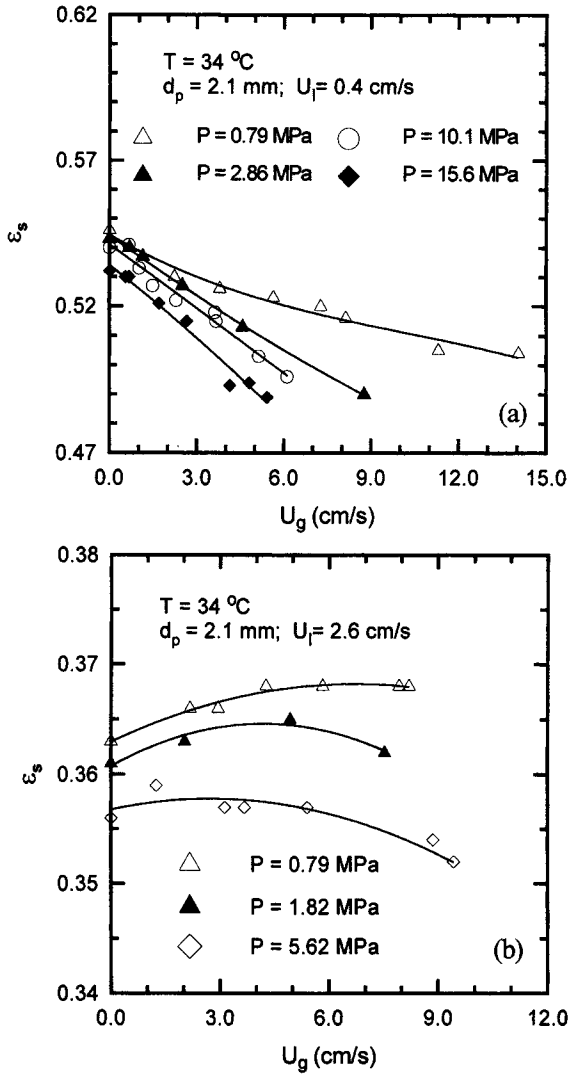

Figure 10. Effects of gas velocity on solids holdup at various pressures and (a) $U_l = 0.4$ cm/s; (b) $U_l = 2.6$ cm/s.

pressure increases at a constant liquid velocity, both the viscosity and density of the liquid phase increases, leading to a smaller solids holdup under the condition of $U_g = 0$. In three-phase fluidized beds, the variations of bubble characteristics with pressure contribute to the bed expansion behavior in two aspects. The decrease in bubble size at high pressures directly reduces the liquid entrainment by the bubble wakes. In addition, the linear liquid velocity (U_l/ϵ_l) increases because of the smaller liquid holdup. The overall effect of the bubble-size reduction is to increase the effective fluidizing liquid velocity in the liquid–solid region, hence resulting in an increased bed expansion or smaller solids holdup.

Heat transfer

Figure 12 shows the variation of the coefficient of heat transfer between the immersed surface and the bed with the liquid holdup for liquid–solid fluidized beds under ambient conditions. It is seen in the figure that the heat-transfer coefficient in the bed of 3-mm particles is larger than that in the

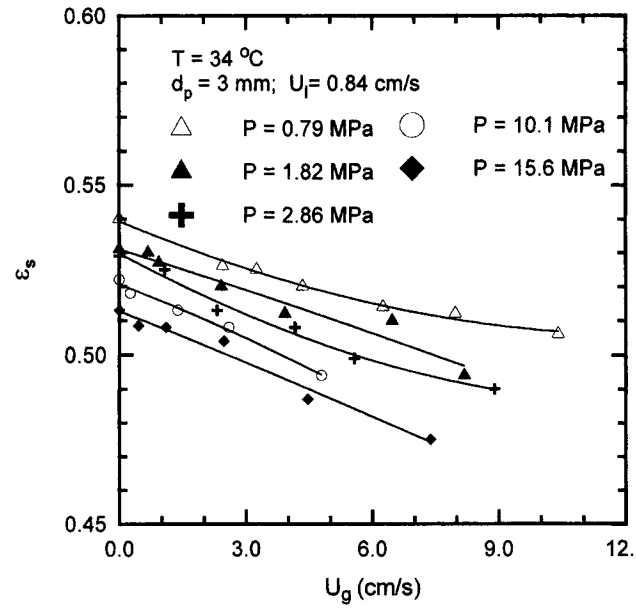

Figure 11. Effect of gas velocity on solids holdup at various pressures.

bed of 2-mm particles for a given liquid voidage. For both particles, the heat-transfer coefficient exhibits maximum values at a voidage of approximately 0.62. The existence of a maximum is a result of the counteracting effects of an increase in the liquid velocity and a decrease in the solids concentration. A similar result was reported on the heat transfer in liquid–solid fluidized beds previously (Wasmund and Smith, 1967; Richardson et al., 1976).

The variations of the heat-transfer coefficient with the gas and liquid velocities at a high pressure are shown in Figure 13. It is seen that upon the introduction of the gas into the

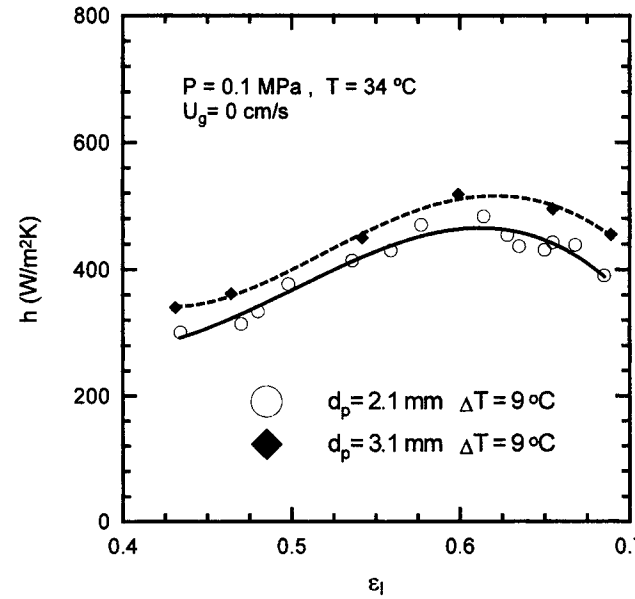

Figure 12. Effect of liquid holdup on heat-transfer coefficient for two sizes of particles in a liquid–solid fluidized bed.

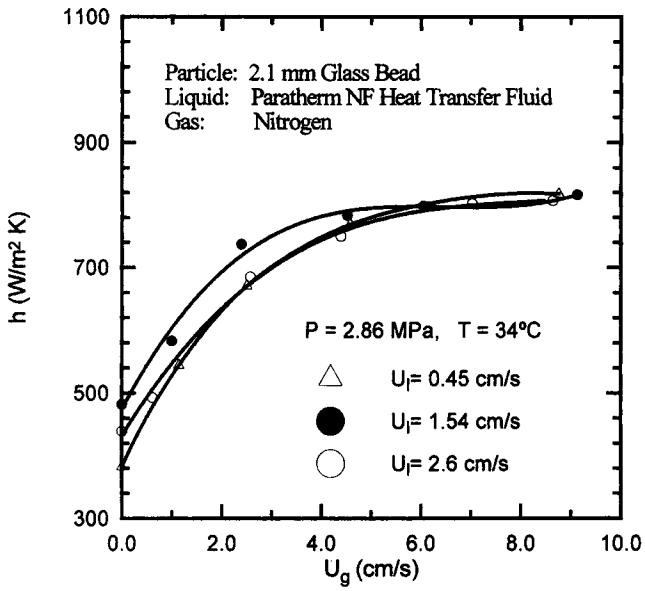

Figure 13. Effects of U_g and U_l on heat-transfer coefficient at a pressure of 2.86 MPa.

liquid–solid fluidized beds the heat transfer is greatly enhanced. The heat-transfer coefficient levels off as the gas velocity continues to increase. The gas velocity appears to have greater effect on the heat transfer compared to the liquid velocity.

A variation in pressure alters the physical properties of the gas and liquid and the hydrodynamics of the bed, yielding a complex effect on heat-transfer behavior in the bed. Previous studies on the heat transfer in three-phase fluidized beds with liquids of different viscosities indicated that liquid viscosity has a negative effect on the heat transfer (Kato et al., 1981; Kang et al., 1985). Since the liquid viscosity increases with pressure (Table 2), the pressure would have a negative effect on the heat transfer. Other liquid physical properties that are less affected by pressure include ρ_l, k_l, and C_{pl} (Reid et al., 1977). Studies on instantaneous heat transfer in liquid and liquid–solid systems upon the introduction of single bubbles revealed the importance of bubble wakes (Kumar et al., 1992). The heat-transfer enhancement by bubbles was found to increase with bubble size due to an increased wake size and wake vortical intensity. When the pressure increases, the bubble size decreases and hence the wake contribution to the heat transfer by single bubbles is reduced. Meanwhile, the decrease in the solids holdup may also yield a smaller heat-transfer coefficient. In chain bubbling systems, Kumar and Fan (1994) reported that the time-averaged heat-transfer coefficient is dependent on bubbling frequency. The heat-transfer coefficient in chain bubbling systems increases with bubbling frequency, due to the intense bubble–wake, bubble–bubble, and bubble–surface interactions. Because the gas holdup and the bubble number density increase significantly with pressure, the frequency of bubble passage over the heating surface increases, which promotes the heat transfer. The effect of pressure on the heat transfer due to the variations in liquid properties and hydrodynamic parameters is summarized in Table 3.

The heat-transfer coefficients of the three-phase fluidized beds at various pressures as a function of the gas velocity are shown in Figure 14. It can be seen from this figure that as the pressure increases, the heat-transfer coefficient increases until a critical pressure is reached, beyond which the heat-transfer rate decreases, independent of the liquid velocity and the particle size. This trend is more apparent in Figure 15 where the heat-transfer coefficient reaches a maximum value at pressures of 6–8 MPa for two particles of 2.1-mm and 3.0-mm glass beads. It is important to note that the point where the pressure effect on the hydrodynamics (Figures 4, 6, and 9) and the heat transfer diminishes occurs in the same pressure range. When the pressure effect on the gas holdup levels off, a further increase in pressure could lead to a decrease in the heat-transfer coefficient (see Table 3). Thus, an increase in gas holdup or frequency of bubble passages over the heating surface could enhance the heat transfer in three-phase fluidized beds. This enhancement is dominant over other factors, such as an increase in liquid viscosity and a decrease in bubble size and solids holdup, that impose a negative effect on the heat transfer as the pressure increases. This is due to the fact that the variation in pressure mainly alters the size and number density of large bubbles. Even a small decrease in the number and size of large bubbles can lead to a significant increase in the gas holdup and the bubble number density in the bed (see Equations 8–11).

Heat-Transfer Mechanism. In liquid–solid fluidization systems, the major factor contributing to the heat transfer is the liquid convection; the particle-convective heat transfer is negligible (Wasmund and Smith, 1967). A mechanistic model, that is, the consecutive film and surface-renewal model originally developed by Wasan and Ahluwalia (1969) for gas–solid and liquid–solid systems has been employed by Kumar and Fan (1994) to account for the heat transfer in three-phase flu-

Table 3. Variations of Various Parameters with Pressure and the Effects on Heat-Transfer Coefficient

Parameters	Effect of Inc. in Parameter Value on Heat-Transfer Coeff.	Effect of Pres. Inc. on Parametric Value	Parametric Effect on Heat-Transfer Coeff. with Inc. in Pres.
μ_l	−	+	−
ρ_l	+	+ (small)	+ (small)
k_l	+	+ (small)	+ (small)
C_{pl}	+	+ (small)	+ (small)
σ	No direct effect	−	No direct effect
d_b	+	−	−
ϵ_g	+	+	+
ϵ_s	+	−	−

Note: +: increase; −: decrease.

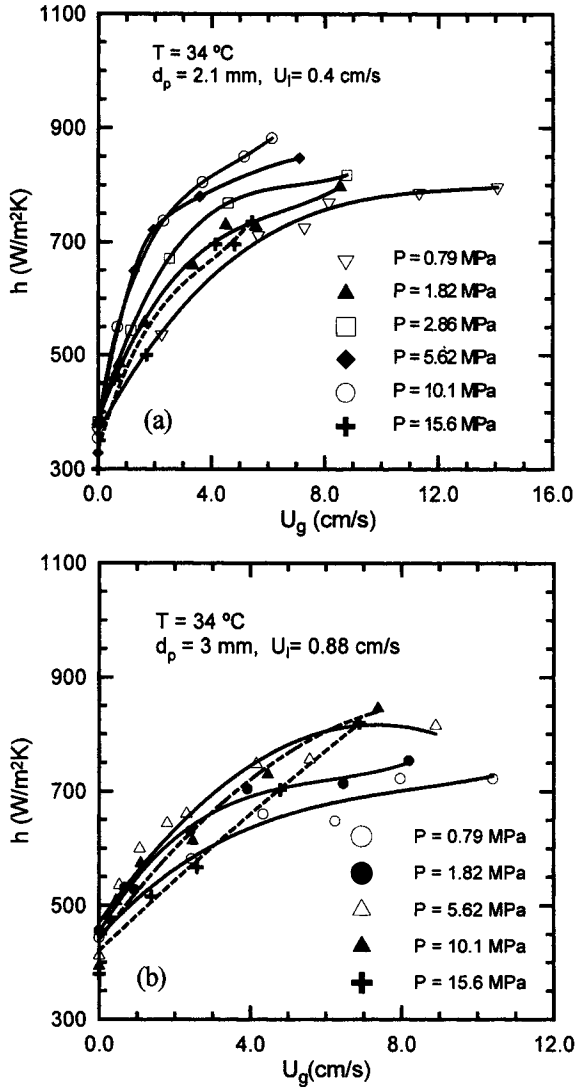

Figure 14. Effects of U_g on the heat-transfer coefficient at various pressures for (a) $d_p = 2.1$ mm; (b) $d_p = 3$ mm.

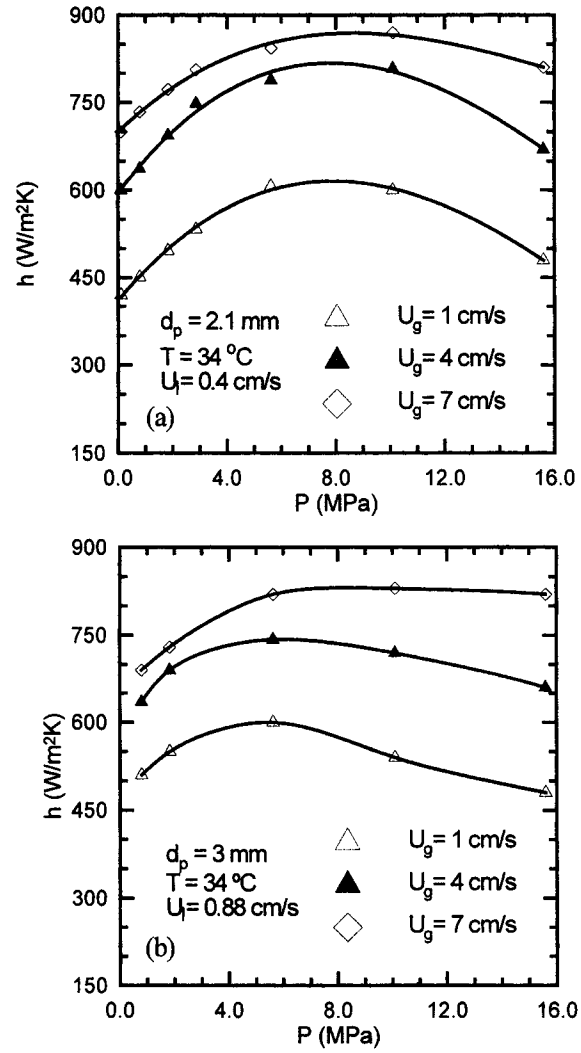

Figure 15. Effect of pressure on heat-transfer coefficient at various values of U_g for (a) $d_p = 2.1$ mm; (b) $d_p = 3$ mm.

idized beds. In this study, the consecutive film and surface-renewal model is extended to examine the heat-transfer behavior at high pressures. Consider that a thin liquid film of thickness δ exists surrounding the heating surface, through which the heat transfer takes place by conduction. The outer surface of the film is continuously renewed with fluid elements induced by the passage of bubbles, in contact with the surface for a time period of θ_c. During the contact, the heat is transferred by the elements through unsteady-state conduction. The time-averaged heat-transfer coefficient from the heating surface to the bed can be expressed in terms of the physical properties of the liquid, the film thickness, δ, and the contact time between the liquid elements and the film, θ_c, as (Wasan and Ahluwalia, 1969)

$$h = \frac{2k_l}{\sqrt{\pi\alpha\theta_c}} + \frac{k_l\delta}{\alpha\theta_c}\left\{\left[1-\mathrm{erf}\left(\frac{\sqrt{\alpha\theta_c}}{\delta}\right)\right]e^{(\alpha\theta_c)/\delta^2}-1\right\}. \quad (12)$$

The contribution of the film resistance to the total heat-transfer resistance can be expressed solely in terms of $(\sqrt{\alpha\theta_c}/\delta)$, as shown in Figure 16. The controlling mechanism of the heat transfer in three-phase fluidized beds at high pressures can be identified when the parameter $(\sqrt{\alpha\theta_c}/\delta)$ is known.

Following the analysis of Kumar and Fan (1994), the order of magnitude of the film thickness can be estimated by

$$\delta = \frac{6.14L}{Re^{3/4}} Pr^{-1/3}, \quad (13)$$

where $Re = \rho_l L U_b/\mu_l$ and the bubble rise velocity, U_b, can be approximated by U_g/ϵ_g. Calculations based on Eq. 13 reveal that δ is typically larger than 0.2 mm in the present high-pressure system.

The contact time between the liquid element and the film is equivalent to that between the bubbles and the film, as bubbles are the source of the liquid element replacement as noted earlier. The contact time between the film and the

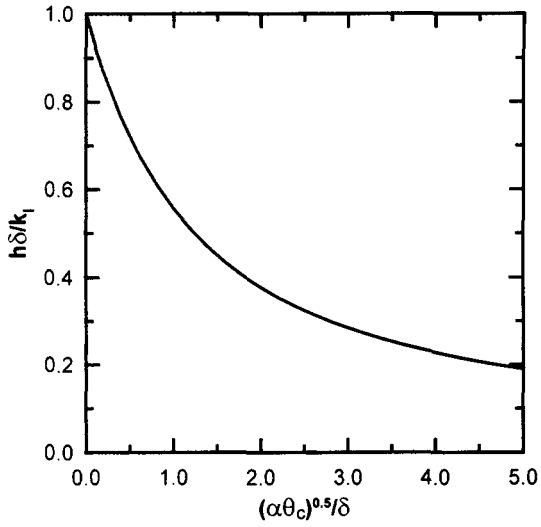

Figure 16. Variation of the parameter $h\delta/k_l$ with parameter $(\alpha\theta_c)^{0.5}/\delta$. (After Wasan and Ahluwalia, 1969.)

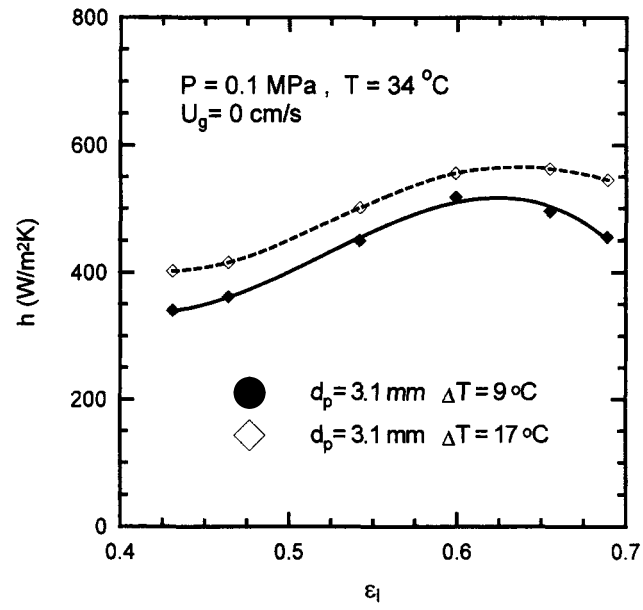

Figure 17. Effect of temperature difference on the heat-transfer coefficient between the heating surface and bed.

bubbles, θ_c, can be evaluated by considering a film of unit width and height. The area occupied by the bubbles is ϵ_g. Therefore, the number of bubbles on the film becomes

$$N_s = \frac{4\epsilon_g}{\pi d_b^2}, \tag{14}$$

and each bubble stays on the surface for a time period of

$$t_c = \frac{1}{U_b}. \tag{15}$$

The contact time, θ_c, is the reciprocal of the collision frequency between the bubbles and the film, that is,

$$\theta_c = \frac{1}{f_c} = \frac{1}{N_s/t_c} = \frac{\pi d_b^2}{4\epsilon_g U_b}. \tag{16}$$

Based on Eq. 16, θ_c decreases as the pressure increases. An alternative method to estimate θ_c is to apply the isotropic turbulence theory (Deckwer, 1980; Suh et al., 1985), as given by

$$\theta_c = \left(\frac{\nu_l}{P_v}\right)^{1/2} = \left\{\frac{\epsilon_l \mu_l}{[(U_l + U_g)(\epsilon_s \rho_s + \epsilon_l \rho_l + \epsilon_g \rho_g) - U_l \rho_l]g}\right\}^{1/2}. \tag{17}$$

Equation 16 gives smaller values of θ_c than does Eq. 17. But θ_c is typically less than 0.02 s from both equations, under the current experimental conditions. Thus, the parameter $(\sqrt{\alpha\theta_c}/\delta)$ is less than 0.2 and, from Figure 16, the film resistance accounts for more than 88% of the total heat-transfer resistance. Thus, it can be stated that the heat transfer in high-pressure three-phase fluidized beds is predominantly determined by the film mechanism. Experimental evidence confirming this point is given in Figure 17, which shows the variation in heat-transfer coefficient when the temperature difference between the heat-transfer surface and the bed is changed. Similar results are found in three-phase fluidized beds. In Figure 17, with an increase in the temperature difference by 8°C while the bulk temperature in the bed remains the same, the temperature of the heating surface increases from 43°C to 51°C. This increase in the heating surface temperature leads to a 25% decrease in the liquid viscosity surrounding the heating surface, which results in the increase in the heat-transfer coefficient at constant superficial liquid velocities. The result of Deckwer et al. (1980) in F–T synthesis slurry bubble columns, that is, the heat-transfer coefficient slightly increases with the heating-surface temperature, can also be illustrated by the film heat-transfer mechanism.

Since the film heat transfer is the controlling heat-transfer mode, the high heat-transfer rate in three-phase fluidized beds can be attributed to the erosion of film induced by bubbles and particles. When the pressure increases, the gas holdup and the bubble number density increase and so does the contact frequency between the bubbles and the film, resulting in more erosion of the film by bubbles. In this manner, the heat-transfer coefficient increases with pressure up to 6–8 MPa. Beyond this pressure range, the gas holdup essentially does not change; an increase in the liquid viscosity and a decrease in the solids holdup yield a decrease in the heat-transfer coefficient when pressure further increases.

Based on the preceding discussion, phase holdups are important to the heat-transfer coefficient in three-phase fluidized beds. The following empirical equation is thus proposed to correlate the data of the heat-transfer coefficient obtained in this study with the gas holdup:

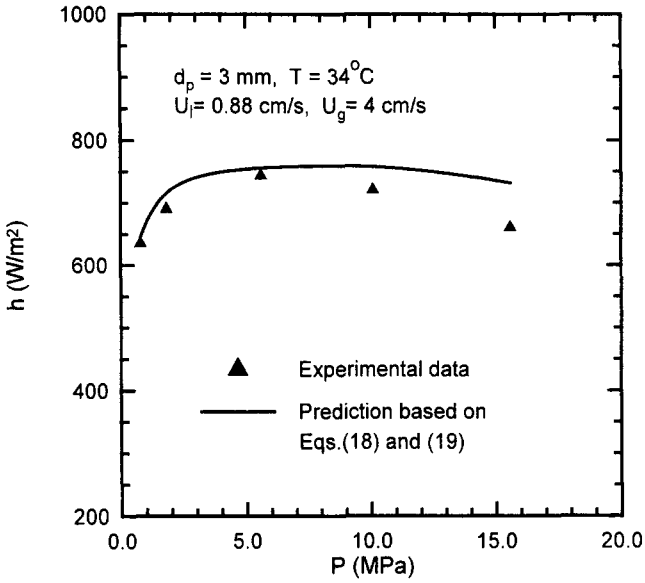

Figure 18. Comparison between experimental data and the prediction based on the correlation.

$$h = h'\epsilon_g^{0.45}\left(\frac{0.396}{U_g^{0.45}} + \frac{0.6768}{U_{pt,0}}\right) \qquad (U_g > 0), \qquad (18)$$

where h' is the heat-transfer coefficient of a liquid–solid fluidized bed with the same solids holdup, and $U_{pt,0}$ is the particle terminal velocity in the fluidizing liquid at the ambient pressure. We can calculate h' by the correlation given below (Richardson et al., 1976):

$$Nu' = 0.67Re^{0.62}Pr^{0.33}\frac{\epsilon_s^{0.38}}{(1-\epsilon_s)}. \qquad (19)$$

In applying Eqs. 18 and 19, the *in situ* liquid physical properties and phase holdups are used with $U_{pt,0}$ based on the properties at the ambient pressure. Figure 18 shows that Eqs. 18 and 19 can correctly predict the pressure effect on the heat-transfer coefficient of three-phase fluidized beds in this work. The average deviation of the prediction from the experimental data is within $\pm 10\%$.

Concluding Remarks

The pressure is found to have a significant effect on the hydrodynamics and heat-transfer characteristics of three-phase fluidized beds. Through the variation of the physical properties of the gas and liquid phases, the pressure affects the bubble size and size distribution and the bubble coalescence and breakup phenomena. Higher pressures yield smaller bubbles and more uniform bubble-size distribution, and thus higher gas velocities are required for the regime transition from dispersed bubbles to the coalesced bubbles. The reduction in bubble size due to increasing pressure also leads to an increase in the gas holdup and a decrease in the liquid and solids holdups. At pressures exceeding 6 MPa, the pressure effect on the hydrodynamic properties is insignificant.

With an increase in pressure, the heat-transfer coefficient increases, reaches a maximum at pressures of 6–8 MPa, and then decreases. The major heat-transfer resistance is found to be within the liquid film surrounding the heat-transfer surface. High heat-transfer coefficients at high pressures arise from the high extent of film erosion induced by the motion of small bubbles. The heat-transfer coefficient at high pressures can be predicted by an empirical correlation, taking into account the phase holdups and the physical properties of the liquid.

Acknowledgment

The work was supported by the National Science Foundation under Grant CTS-9528380.

Notation

A = cross-sectional area of the column, m^2
A_h = Hamaker constant of the liquid, J
a_0 = initial particle acceleration upon the collision between a bubble and a particle, m/s^2
$C_{p,l}$ = heat capacity of the liquid, J/kg·K
d_p = particle diameter, m
$f(d_b)$ = probability distribution function of bubble size, based on the number of bubbles, 1/m
f_c = frequency of contact between the film and bubbles, 1/s
g = gravitational acceleration, m/s^2
h = heat-transfer coefficient in three-phase fluidized beds, W/m^2·K
k = thermal conductivity, W/m·K
l = thickness of the liquid film between two coalescing bubbles, m
L = vertical length of the heating surface, m
N_s = number of bubbles per unit area
Nu' = Nusselt number in liquid–solid fluidized beds, $h'd_p/k_l$
P_d = dynamic pressure in three-phase fluidized beds, Pa/m
P_v = energy dissipation per unit volume, W/m^3
q = heat flux, W/m^2
Pr = Prandtl number, $C_{p,l}\mu_l/k_l$
R = frontal radius of curvature for a spherical cap bubble, m
R_d = radius of the contacting circle between two coalescing bubbles, m
Re = Reynolds number, $\rho_l L U_b/\mu_l$, in Eq. 15; Reynolds number, $\rho_l d_p U_b/\mu_l$, in Eq. 21
t = time, s
T_b = temperature of the bed, K
T_s = temperature of the heating surface, K
U_g = superficial gas velocity, m/s
U_l = superficial liquid velocity, m/s
U_{p0} = initial descending velocity of the particle, m/s
V_R = ratio of the film-thinning velocity at a given pressure to that at the ambient pressure
W_s = weight of particles in the bed, kg
z = distance from the distributor in the bed, m
α = thermal diffusivity, $k_l/(C_{p,l}\rho_l)$, m^2/s
μ = viscosity, Pa·s
ν_l = kinematic viscosity of the liquid, m/s
ρ = density, kg/m^3
σ = surface tension, N/m
τ = total sampling time, s

Literature Cited

Baker, C. G. J., E. R. Armstrong, and M. A. Bergougnou, "Heat Transfer in Three-Phase Fluidized Beds," *Powder Technol.*, **21**, 195 (1978).

Bellman, R., and R. H. Pennington, "Effect of Surface Tension and Viscosity on Taylor Instability," *Q. Appl. Math.*, **51**, 151 (1954).

Bhatia, V. K., and N. Epstein, "Three-Phase Fluidization: A Generalized Wake Model," *Fluidization and Its Applications*, H. Angelino,

J. P. Couderc, H. Gibert, and C. Laguerie, eds., Cepadues-Editions, Toulouse (1974).
Blum, D., and J. J. Toman, "Three-Phase Fluidization in a Liquid Phase Methanator," *AIChE Symp. Ser.*, **73**(161), 115 (1977).
Chaudhari, R. V., and H. Hofmann, "Coalescence of Gas Bubbles in Liquids," *Rev. Chem. Eng.*, **10**, 131 (1994).
Chen, Y.-M., and L.-S. Fan, "On the Criteria of Rayleigh-Taylor Instability at a Curved Interface by a Local Force Balance," unpublished results (1988).
Chen, Y.-M., and L.-S. Fan, "Bubble Breakage Mechanisms due to Collision with a Particle in a Liquid Medium," *Chem. Eng. Sci.*, **44**, 117 (1989).
Clark, K. N., "The Effect of High Pressure and Temperature on Phase Distributions in a Bubble Column," *Chem. Eng. Sci.*, **45**, 2301 (1990).
Darton, R. C., and D. Harrison, "Gas and Liquid Hold-up in Three-Phase Fluidization," *Chem. Eng. Sci.*, **30**, 581 (1975).
Deckwer, W.-D., Y. Louisi, A. Zaidi, and M. Ralek, "Hydrodynamic Properties of the Fisher-Tropsch Slurry Process," *Ind. Eng. Chem. Process Des. Dev.*, **19**, 699 (1980).
Deckwer, W.-D., "On the Mechanism of Heat Transfer in Bubble Column Reactors," *Chem. Eng. Sci.*, **35**, 1341 (1980).
El-Temtamy, and N. Epstein, "Contraction or Expansion of Three-Phase Fluidized Beds Containing Fine/Light Solids," *Can. J. Chem. Eng.*, **57**, 520 (1979).
Fan, L.-S., *Gas-Liquid-Solid Fluidization Engineering*, Butterworths, Stoneham, MA (1989).
Fan, L.-S., and K. Tsuchiya, *Bubble Wake Dynamics in Liquids and Liquid-Solid Suspensions*, Butterworth-Heinemann, Stoneham, MA (1990).
Henriksen, H. K., and K. Ostergaard, "On the Mechanism of Break-up of Large Bubbles in Liquids and Three-phase Fluidized Beds," *Chem. Eng. Sci.*, **29**, 626 (1974).
Idogawa, K., K. Ikeda, T. Fukuda, and S. Morooka, "Formation and Flow of Gas Bubbles in a Single Orifice or Nozzle Gas Distributor," *Chem. Eng. Commun.*, **59**, 201 (1987).
Jiang, P., D. Arters, and L.-S. Fan, "Pressure Effects on the Hydrodynamic Behavior of Gas-Liquid-Solid Fluidized Beds," *Ind. Eng. Chem. Res.*, **31**, 2322 (1992).
Jiang, P., X. Luo, T.-S. Lin, and L.-S. Fan, "Flow Visualization of High Pressure and High Temperature Three-Phase Fluidization—Incipient Fluidization," *Fluidization VIII: Proc. Int. Conf. on Fluidization*, Tours, France, p. 433 (1995).
Jiang, P., X. Luo, T.-S. Lin, and L.-S. Fan, "High Temperature and High Pressure Three-Phase Fluidization-Bed Expansion Phenomena," *Powder Technol.*, **90**, 103 (1997).
Kang, Y., I. S. Suh, and S. D. Kim, "Heat Transfer Characteristics of Three-Phase Fluidized Beds," *Chem. Eng. Commun.*, **34**, 1 (1985).
Kato, Y., K. Uchida, and S. Morooka, "Liquid Holdup and Heat Transfer Coefficient Between Bed and Wall in Liquid-Solid and Gas-Liquid-Solid Fluidized Beds," *Powder Technol.*, **28**, 173 (1981).
Kato, Y., K. Uchida, T. Kago, and S. Morooka, "Heat Transfer Coefficient between an Inserted Vertical Tube and a Three-Phase Fluidized Bed," *Kagaku Kogaku Ronbunshu*, **10**, 537 (1984).
Kim, S. D., Y. Yang, and H. K. Kwon, "Heat Transfer Characteristics of Two- and Three-Phase Slurry Fluidized Beds," *AIChE J.*, **32**, 1397 (1986).
Kim, S. D., and A. Laurent, "The State of Knowledge on Heat Transfer in Three-Phase Fluidized Beds," *Int. Chem. Eng.*, **31**, 284 (1991).
Kumar, S., K. Kusakabe, K. Raghunathan, and L.-S. Fan, "Mechanism of Heat Transfer in Bubbly Liquid and Liquid-Solid Systems: Single Bubble Injection," *AIChE J.*, **38**, 733 (1992).
Kumar, S., K. Kusakabe, and L.-S. Fan, "Heat Transfer in Three-Phase Fluidized Beds Containing Low-Density Particles," *Chem. Eng. Sci.*, **48**, 2407 (1993a).
Kumar, S., K. Kusakabe, and L.-S. Fan, "Heat Transfer in Three-Phase Fluidization and Bubble Columns with High Gas Holdups," *AIChE J.*, **39**, 1399 (1993b).
Kumar, S., and L.-S. Fan, "Heat-Transfer Characteristics in Viscous Gas-Liquid and Gas-Liquid-Solid Systems," *AIChE J.*, **40**, 745 (1994).
LaNauze, R. D., and I. J. Harris, "Gas Bubble Formation at Elevated System Pressures," *Trans. Inst. Chem. Eng.*, **52**, 337 (1974).
Magiliotou, M., Y.-M. Chen, and L.-S. Fan, "Bed-immersed Object Heat Transfer in a Three-Phase Fluidized Bed," *AIChE J.*, **34**, 1043 (1988).
Massimilla, L., N. Majuri, and P. Signorini, "Sull'assorbimento di Gas in Sistema: Solido-Liquido, Fluidizzato," *La Ric. Sci.*, **29**, 1934 (1954).
Michelsen, M. L., and K. Ostergaard, "Hold-up and Fluid Mixing in Gas-Liquid Fluidized Beds," *Chem. Eng. J.*, **1**, 37 (1970).
Reid, R. C., J. M. Prausnitz, and T. K. Sherwood, *The Properties of Gases and Liquids*, McGraw-Hill, New York (1977).
Richardson, J. F., M. N. Roman, and K. J. Shakiri, "Heat Transfer from Immersed Surfaces in Liquid Fluidized Beds," *Chem. Eng. Sci.*, **31**, 619 (1976).
Sagert, N. H., and M. J. Quinn, "Influence of High-pressure Gases on the Stability of Thin Aqueous Films," *J. Colloid Int. Sci.*, **61**, 279 (1977).
Sagert, N. H., and M. J. Quinn, "Surface Viscosities at High Pressure Gas-Liquid Interfaces," *J. Colloid Int. Sci.*, **65**, 415 (1978).
Saxena, S. C., R. Vadivel, and A. C. Saxena, "Hydrodynamic and Heat Transfer Characteristics of Bubble Columns Involving Fine Powders," *Powder Technol.*, **59**, 25 (1989).
Stewart, P. S. B., and J. Davidson, "Three-Phase Fluidization: Water, Particles, and Air," *Chem. Eng. Sci.*, **19**, 319 (1964).
Suh, I. S., G. T. Jin, and S. D. Kim, "Heat Transfer Coefficients in Three-Phase Fluidized Beds," *Int. J. Multiphase Flow*, **11**, 255 (1985).
Tarmy, B., M. Chang, C. Coulaloglou, and P. Ponzi, "Hydrodynamic Characteristics of Three Phase Reactors," *Chem. Eng.* (Oct. 18, 1984).
Vrij, A., "Possible Mechanism for the Spontaneous Rupture of Thin, Free Liquid Films," *Disc. Farad. Soc.*, **42**, 23 (1966).
Wallis, G. B., *One-Dimensional Two-Phase Flow*, McGraw-Hill, New York (1969).
Wasan, D. T., and M. S. Ahluwalia, "Consecutive Film and Surface Renewal Mechanism for Heat or Mass Transfer from a Wall," *Chem. Eng. Sci.*, **24**, 1535 (1969).
Wasmund, B., and J. W. Smith, "Wall to Fluid Heat Transfer in Liquid Fluidized Beds: 2," *Can. J. Chem. Eng.*, **45**, 156 (1967).

Manuscript received Feb. 3, 1997, and revision received May 13, 1997.